Supplementary Materials

Revealing energy storage mechanism of $CsPbBr_3$ perovskite for ultra-stable symmetric supercapacitors

Le Pang, Minh Tam Hoang, Anthony P. O'Mullane, Hongxia Wang

School of Chemistry and Physics, Faculty of Science, Queensland University of Technology (QUT), Brisbane, QLD 4001, Australia.

Correspondence to: Prof. Hongxia Wang, School of Chemistry and Physics, Faculty of Science, Queensland University of Technology (QUT), Brisbane, QLD 4001, Australia. E-mail: hx.wang@qut.edu.au

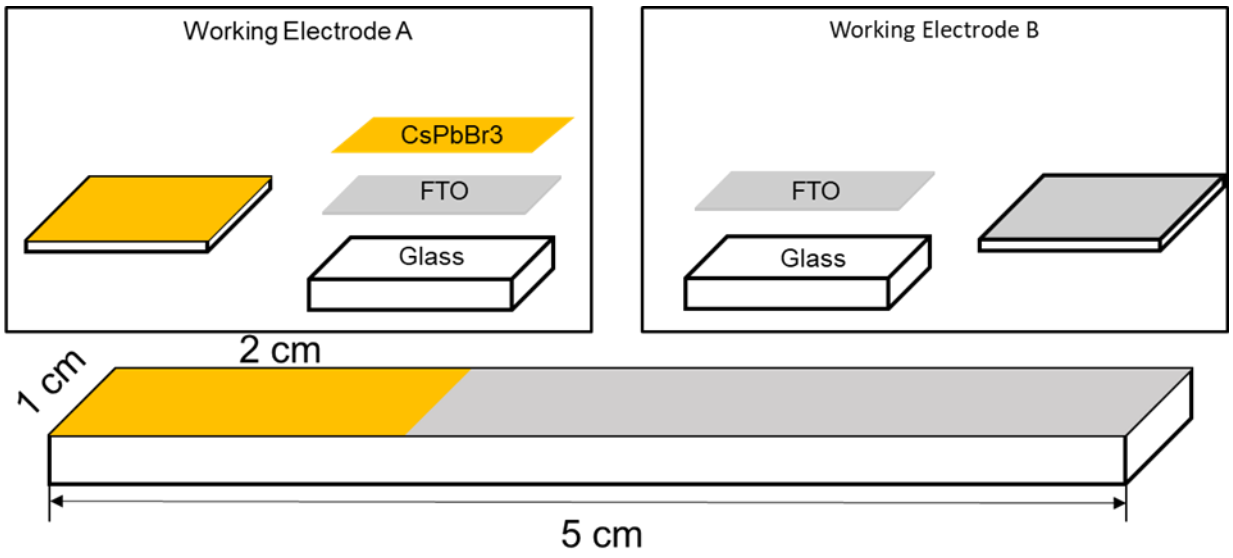

Figure S1: Schematic of the layered structure of $CsPbBr_3$ electrode and FTO substrate.

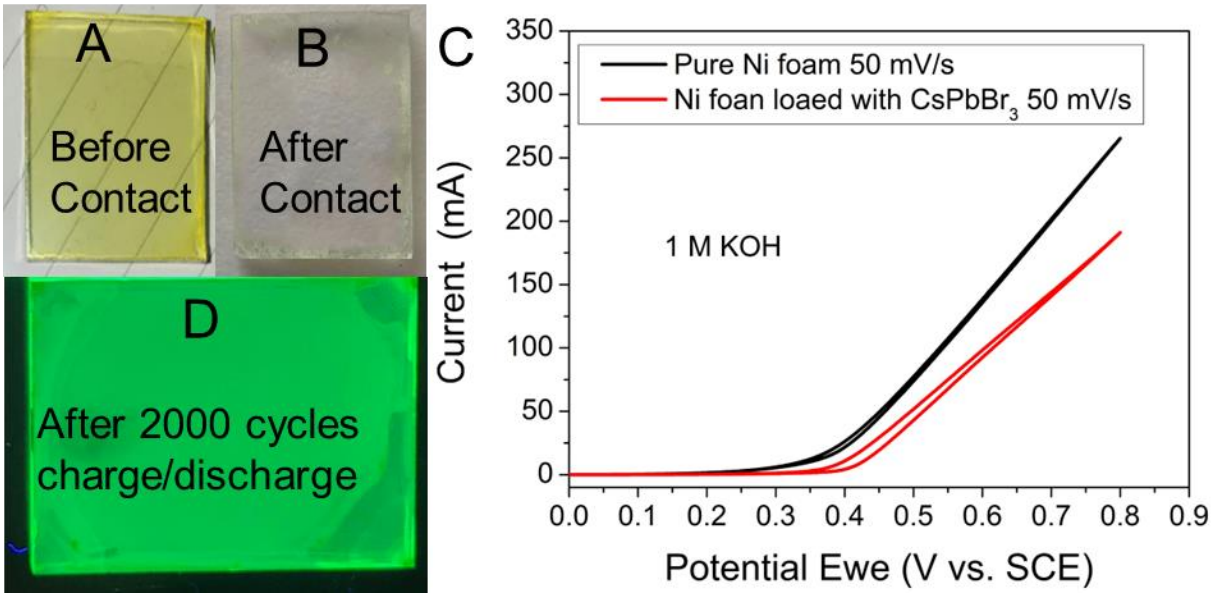

Figure S2. A: the view of the $CsPbBr_3$ film on FTO under normal light before contact with 1 M KOH electrolyte. B: the view of the $CsPbBr_3$ film on FTO under normal light after contact with 1 M KOH electrolyte C: the CV curves of $CsPbBr_3$ on Ni foam in 1 M KOH electrolyte. D: the view of the $CsPbBr_3$ electrode under UV light after 2000 cycles of charge and discharge in $TBAPF_6$ electrolyte.

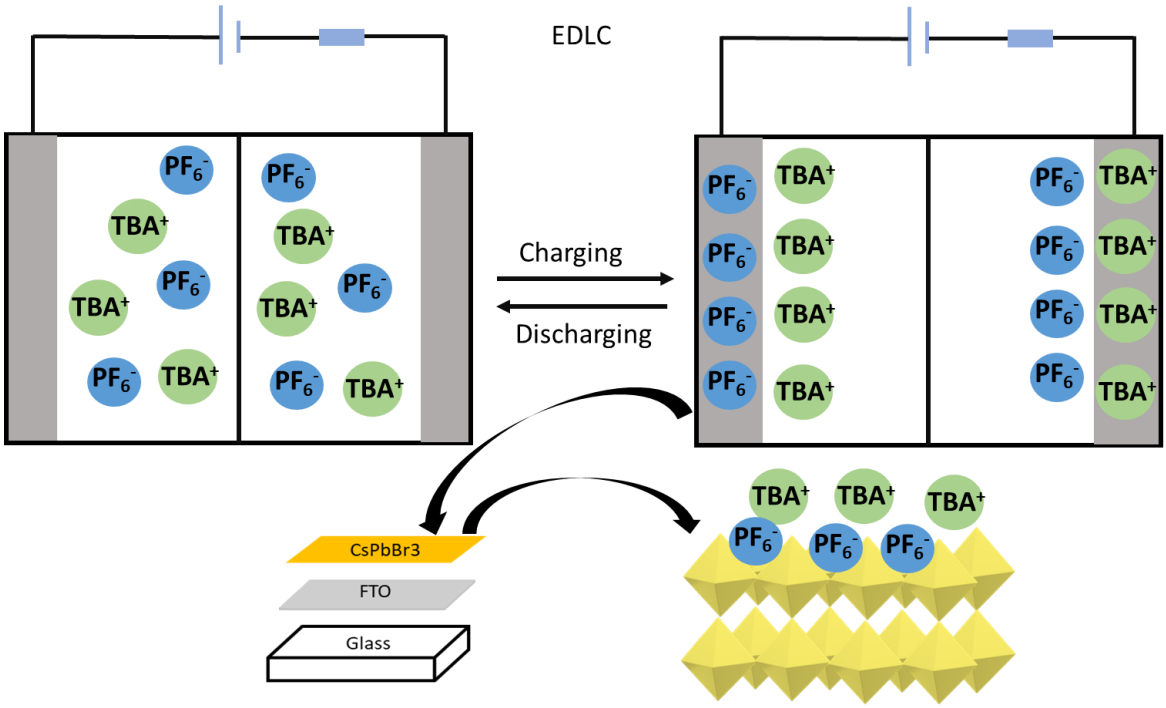

Figure S3. Schematic diagram of the EDLC behaviour of $TBAPF_6$ on the surface of $CsPbBr_3$ electrode.

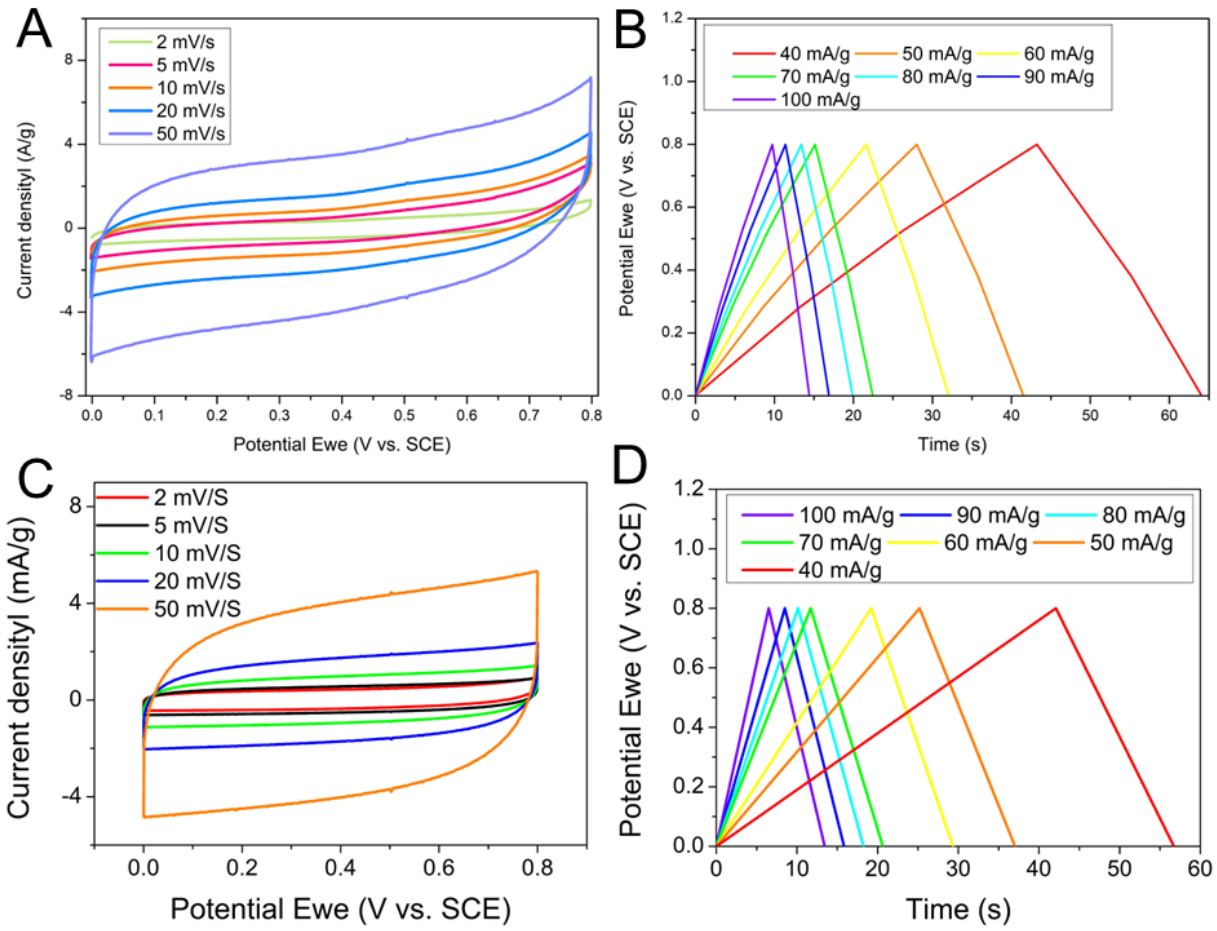

Figure S4. A: the CV curves of CsPbBr3 electrode in 1 M $TBAPF_6$ at different scan rates under N_2 flow. B: the charge and discharge curves of the $CsPbBr_3$ electrode in 1 M $TBAPF_6$ at different current densities under N_2 flow. Figure 4. C: the CV curves of $CsPbBr_3$ electrode in 1 M $TBAPF_6$ at different scan rates in the air. D: the charge and discharge curves of the $CsPbBr_3$ electrode in 1 M $TBAPF_6$ at different current densities in the air.

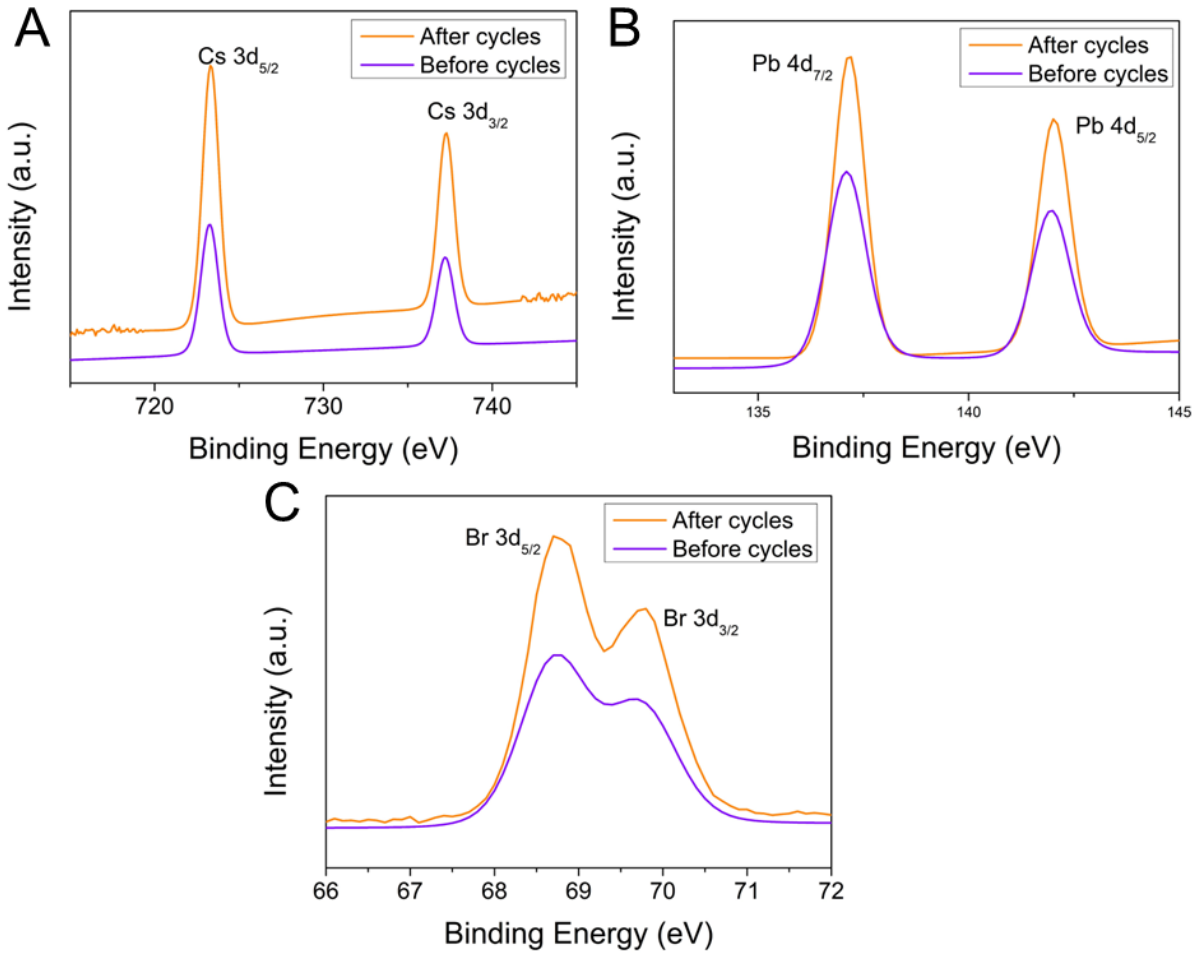

Figure S5. A: High-resolution XPS scans of elements Cs on the $CsPbBr_3$ electrode before and after electrochemical cycling tests. B: High-resolution XPS scans of elements Pb on the $CsPbBr_3$ electrode before and after electrochemical cycling tests. C: High-resolution XPS scans of elements Br on the $CsPbBr_3$ electrode before and after electrochemical cycling tests. The Ar etching was used to remove the $TBAPF_6$ covered on the $CsPbBr_3$ electrode.

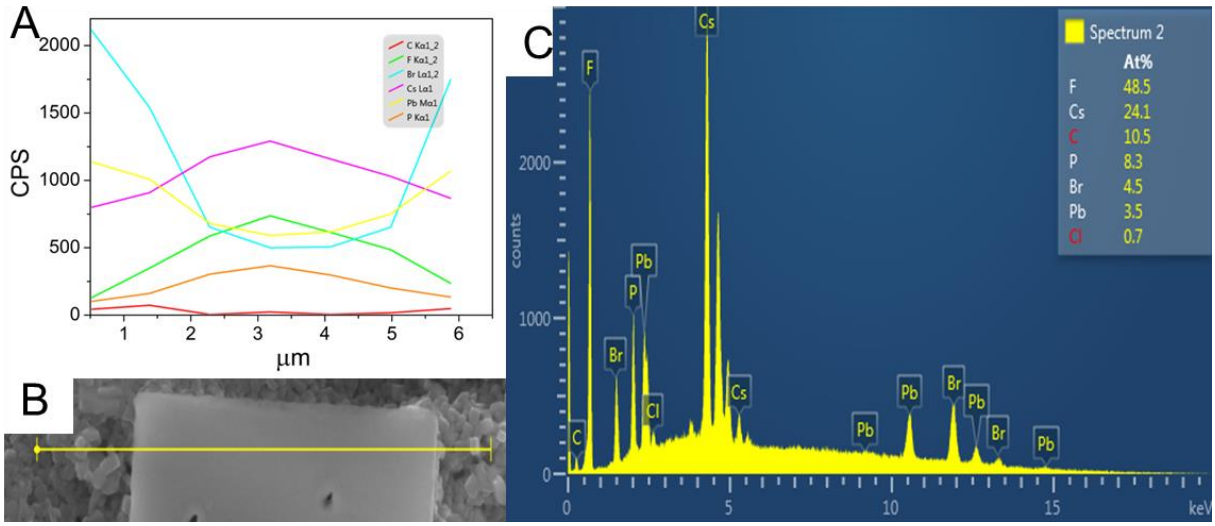

Figure S6. A: the atomic ratio of different elements and their peaks' intensity, correspond to EDS mapping in Figure 5. B: the SEM line scan of the SS-0.1 after the electrochemical test. C: orientation and area of linear scan.

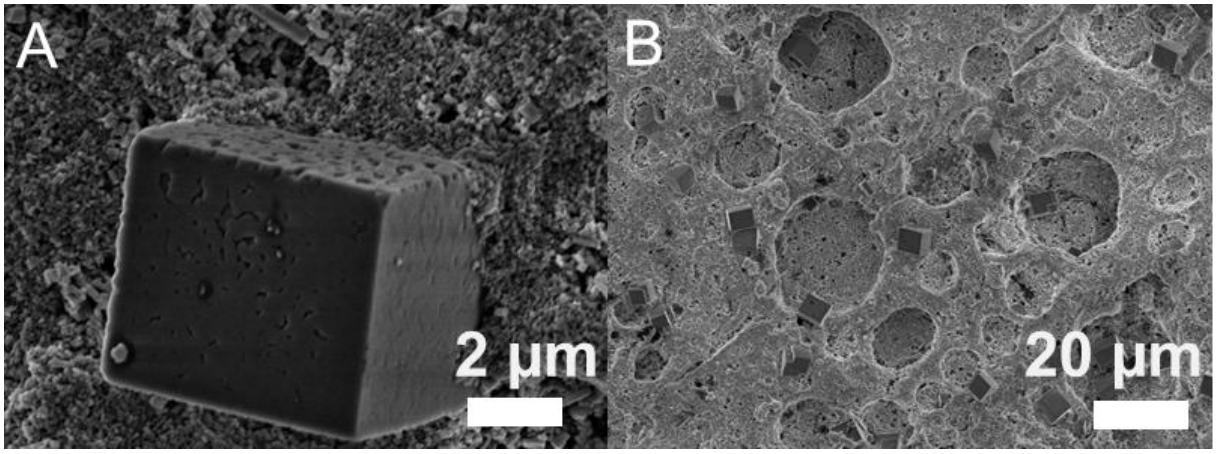

Figure S7. The SEM of the $CsPbBr_3$ electrode after some CV scans at different magnifications A and B.

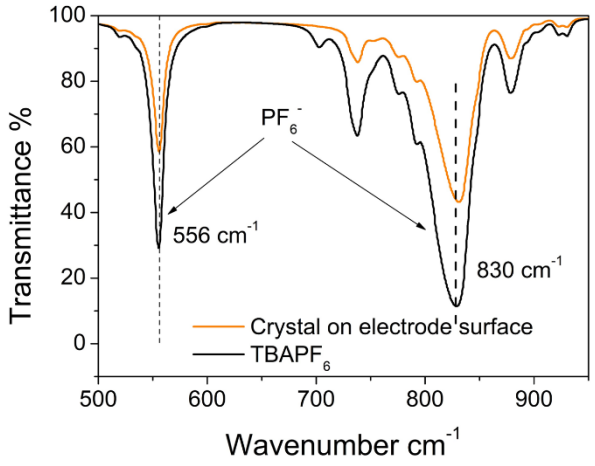

Figure S8. FTIR of $CsPbBr_3$ crystal obtained from $CsPbBr_3$ electrode in SS-1after 2000 cycles of charge and discharge.

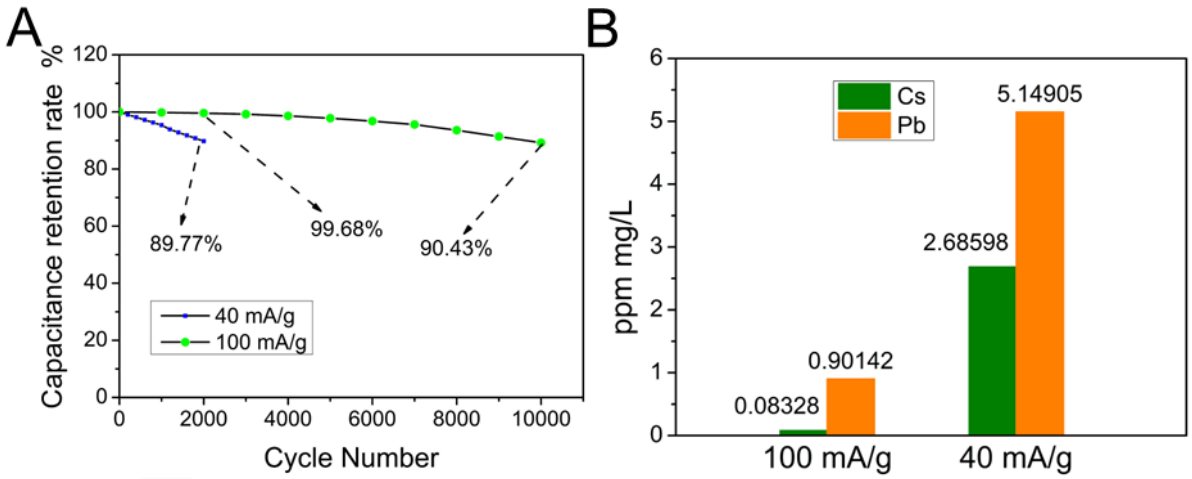

Figure S9. A: Cycling stability of SS-1 after 2000 and 10000 cycles at a current density of 40 mA/g and 100 mA/g. **B:** ICP-MS results of SS-1 after 2000 cycles of charge/discharge af 100 mA/g and 40 mA/g.

Characterization of the $CsPbBr_3$ nanocrystals

The morphology images of the as-synthesized $CsPbBr_3$ nanomaterial measured by SEM and TEM are shown in Figure S10. The synthesized $CsPbBr_3$ nanocrystals adopt a cubic shape as shown in Figure S10A. The high-resolution TEM image (Figure S10B) shows the lattice fringes of the cubic nanocrystals with an interplanar spacing of 0.58 nm, which corresponds to the (100) plane of cubic $CsPbBr_3$.[1], [2] Figure S1C shows the top view of the $CsPbBr_3$ electrode. It is noted that the particle sizes of the $CsPbBr_3$ nanocrystals in Figure S10B (TEM)

are small due to the sonication process. On the other hand, the $CsPbBr_3$ will aggregate to form larger particles due to the effect of particle fusion and coarsening, which is commonly observed in the thin film fabrication and SEM sample preparation process. [3] The cross-section SEM image of the $CsPbBr_3$/FTO/glass electrode in Figure S10D indicates that the $CsPbBr_3$ layer has a thickness of around 700 nm.

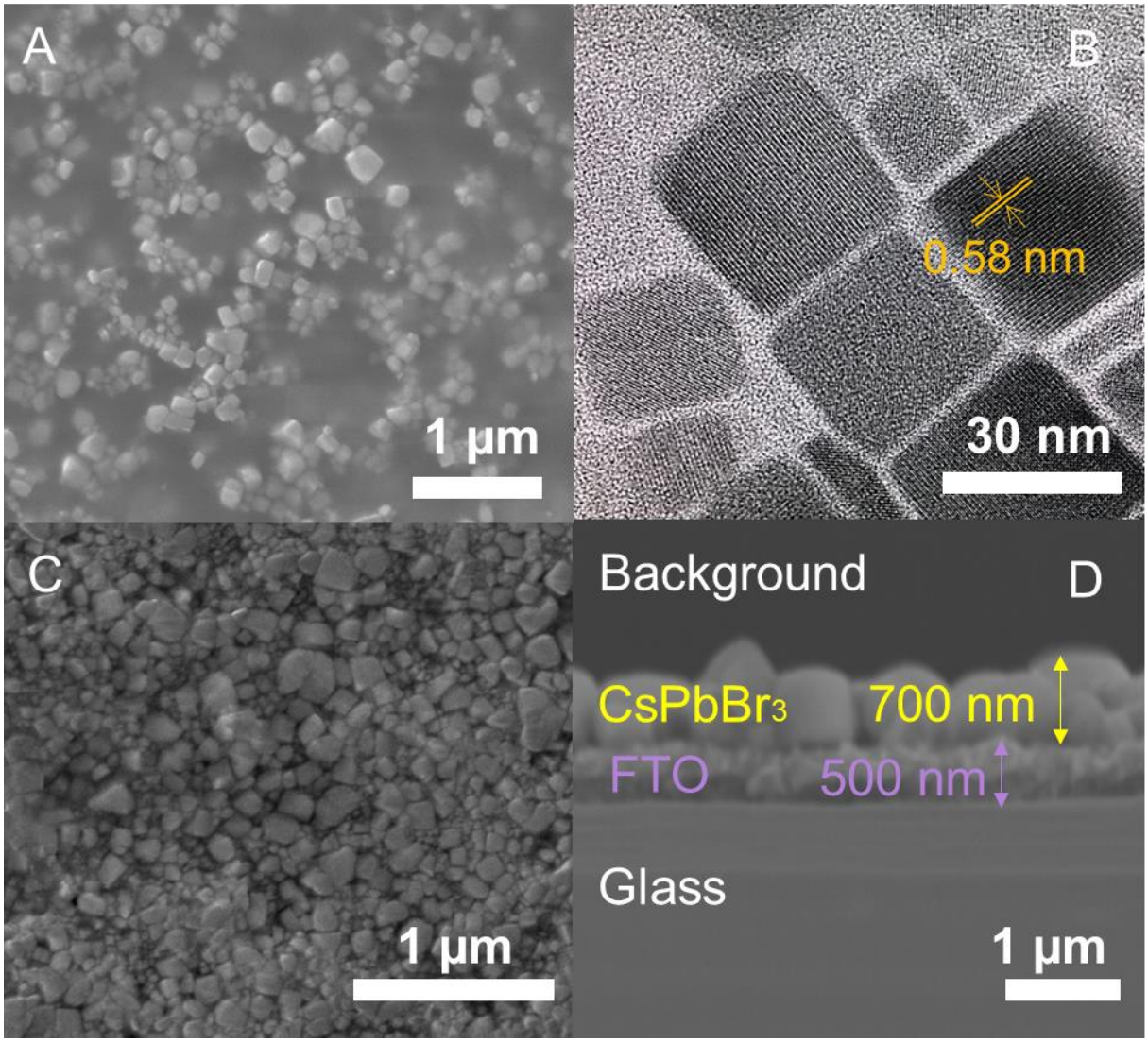

Figure S10. A: the SEM of as-synthesized $CsPbBr_3$ nanocrystals. B: the TEM of as-synthesized $CsPbBr_3$ nanocrystals. C: the top view of $CsPbBr_3$ electrode deposited on FTO glass under SEM. D: the cross-section view of $CsPbBr_3$ electrode deposited on FTO glass under SEM.

The specific surface area of $CsPbBr_3$ nanocrystals was measured in the TriStar II 3020 by argon gas at 87.29 K. Figure S11 A shows the argon sorption isotherm curve (A) of $CsPbBr_3$ belonging to type III according to IPUAC classification. The adsorbent-adsorbate interactions

are relatively weak, and the argon molecules are clustered around the most favourable sites on the surface of our materials, indicating $CsPbBr_3$ is a nonporous or macroporous solid. Figure S11 B shows pore size distribution (B) of $CsPbBr_3$ the majority of the pores of the materials have sizes in the range of 1–4 nm. The BET surface area is 2.0760 ± 0.0131 m^2/g and the Langmuir surface area is 6.0516 ± 0.6486 m^2/g. The correlation coefficient of BET and Langmuir analysis is 0.996. and 0.983 respectively. To the best of our knowledge, this is the first time that the BET of CsPbBr3 perovskite nanocrystals is obtained. Although, there is no relevant literature value that can be compared so far, it is possible that the high capacitance of our materials benefits from the higher specific surface area than the other materials listed in Table S1.

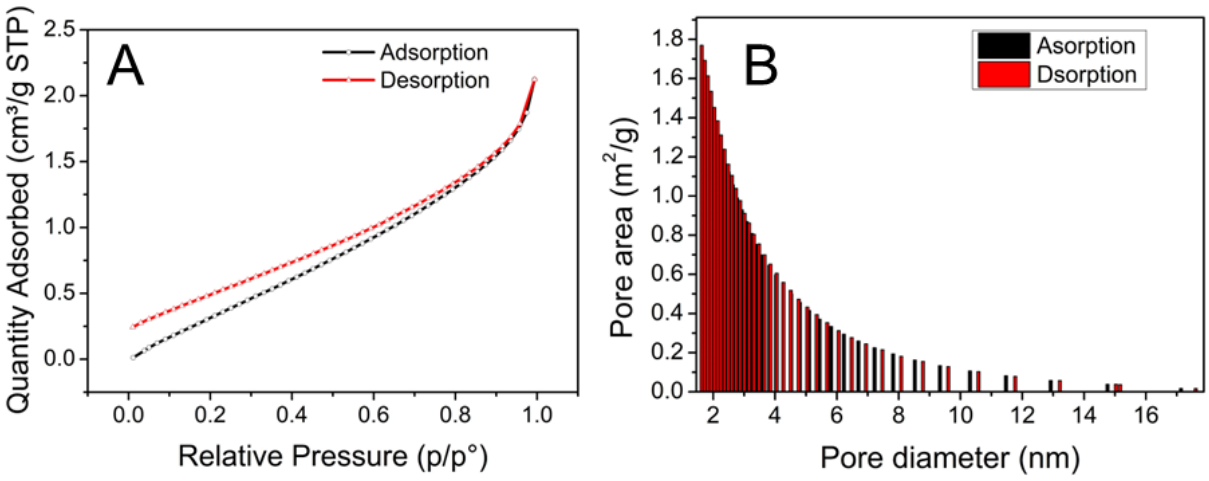

Figure S11. A: Argon adsorption isotherm at 87.29 K. **B:** Pore size distribution with argon gas adsorption at 87.29 K.

XRD was then used to determine the material's crystallographic structure. The peaks at 2θ = 37.79, 30.64, 26.48, 21.43 and 15.06 degrees in the XRD pattern are consistent with the standard diffraction pattern of cubic $CsPbBr_3$ (PDF ID 00-054-0752) (Figure S12A) and other reports in the literature.[4], [5], [6], [7] UV-Vis spectroscopy and photoluminescence spectroscopy (PL) were used to determine the optical properties of the as-synthesized $CsPbBr_3$. The observed onset absorption at 525 nm with a peak at 505 nm in the UV-vis spectrum and a PL photoemission peak at 510 nm are consistent with that of $CsPbBr_3$ (Figure S12B).[8] The bandgap of $CsPbBr_3$ is 2.34 eV which was obtained by fitting the Tauc plot curve of the UV-Vis spectrum (Figure S12C) is consistent with the band gap of bulk $CsPbBr_3$, which means that quantum confinement is negligible due to the large size of the synthesized $CsPbBr_3$ nanocrystal.[8]

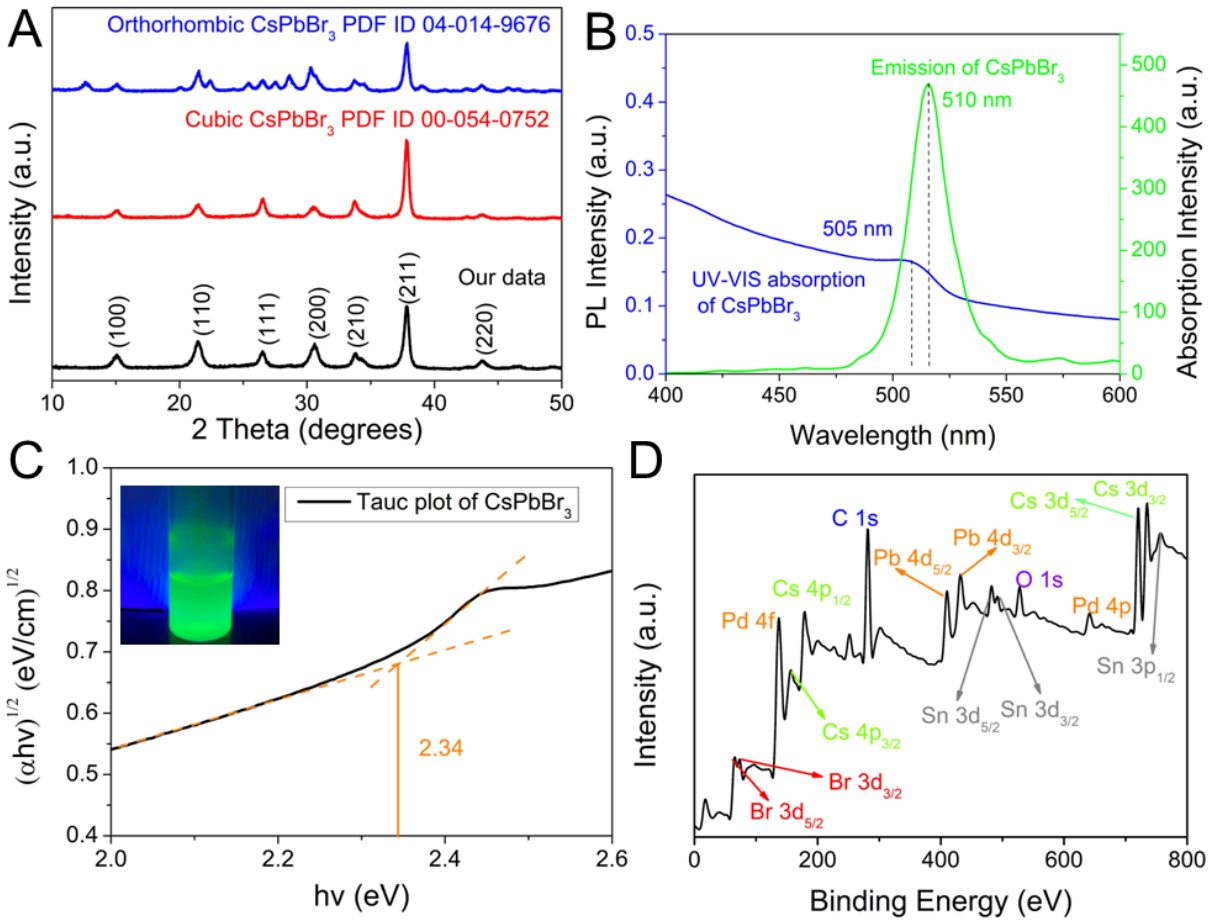

Figure S12. A: XRD spectrum of synthesized $CsPbBr_3$. B: UV-VIS absorption and PL emission of synthesised $CsPbBr_3$. C: Tauc plot and Fluorescence of synthesised $CsPbBr_3$. D: the XPS wide scan of $CsPbBr_3$.

The chemical composition of the materials was measured by XPS and EDS respectively. The XPS (Figure S12D and Figure S13) survey scan confirms the existence of Cs, Pb and Br in the surface of the as-synthesized material with an atomic ratio 1 : 0.97 : 2.82 , which is close to the expected stoichiometric ratio of 1 : 1 : 3 for $CsPbBr_3$. The signals of O, C, and Sn detected in the wide scan (Figure S12D) are attributed to the organic ligand (oleic acid and oleylamine) on the surface of the $CsPbBr_3$ nanocrystals and the FTO substrate since the FTO may not be entirely covered by the $CsPbBr_3$ film. Figure S13A shows two peaks at a binding energy of 723.3 eV and 737.3 eV, which can be assigned to the $3d_{3/2}$ and $3d_{5/2}$ core levels of Cs, respectively. The two peaks at binding energies of 137.1 eV and 142.0 eV are assigned to Pb $3f_{3/2}$ and $3f_{5/2}$ (Figure S13B), whereas peaks for Br $3d_{3/2}$ and $3d_{5/2}$ occur at binding energies of 68.7 eV and 69.7 eV, respectively (Figure S13C).[9], [10], [11], [12] The element composition of

the bulk $CsPbBr_3$ nanocrystals measured by EDS (Figure S13D) also confirms that the atomic ratio of Cs, Pb, and Br is close to 1 : 1 : 3 (i.e. 1 : 1.16 : 2.72).

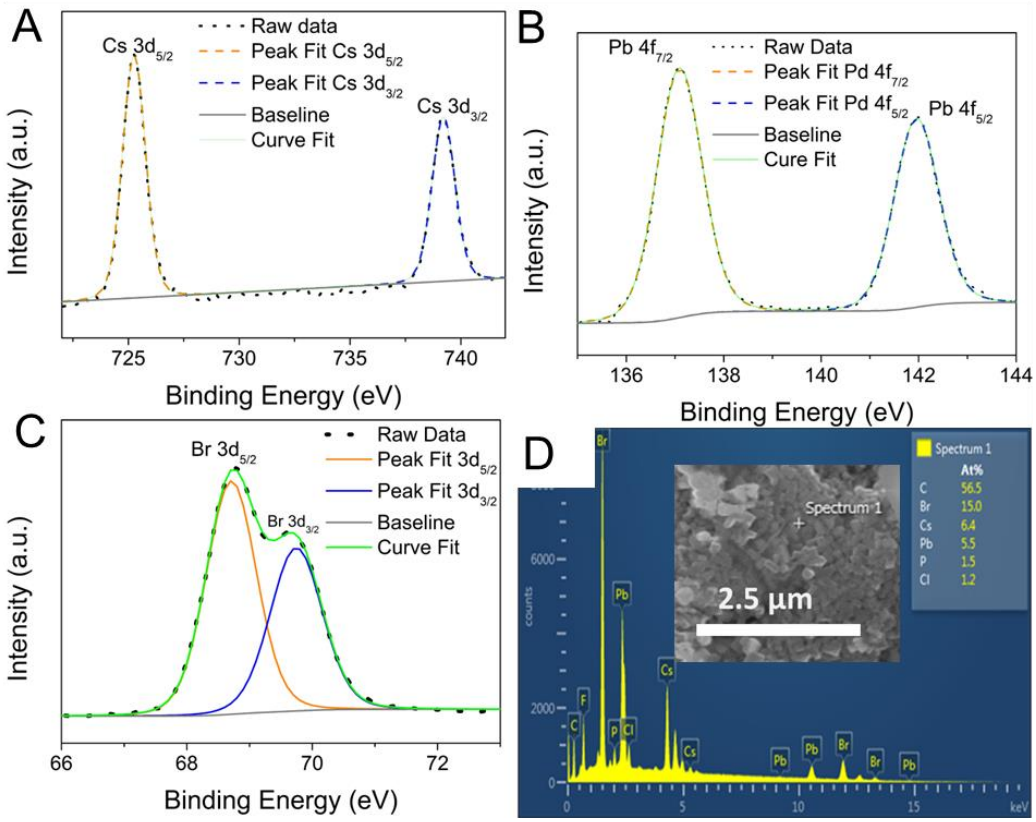

Figure S13. XPS spectrum of synthesised $CsPbBr_3$. A: XPS narrow scan of Cs. B: XPS narrow scan of Pb. C: XPS narrow scan of Br. D: EDS point scan of synthesised $CsPbBr_3$ and the SEM image at corroding position.

Table S1. The performance of other perovskite electrode material in supercapacitor.

	Electrode material	Potential window	Capacitance	Stability	Retention rate	Reference
Our work	$CsPbBr_3$	0–1 V	264 mF/cm 528 mF/g	10000 cycles	90.43 %	This work
Previous work	$CsPbI_3$	0–0.7 V	7.23 mF/cm	1000 cycles	65.5 %	[13]

	$MAPbI_3$	0–0.6 V	21.5 µF/cm	1000 cycles	98.34 %	[14]
	$MAPbI_3$	0–0.6 V	6.95 µF/cm	15000 cycles	82.6 %	[15]
	$(CH_3NH_3)_3Bi_2I_9$	0–0.6 V	5.5 mF/cm	10000 cycles	84.8 %	[16]
	$(CN_2SH_5)_3BiI_6$	0–0.6 V	3.32 F/cm	N/A	N/A	[17]

Table S2. Standard deviation and residual standard deviation of ICP-MS results of SS-0.1 and SS-1 after 2000 cycles of charge/discharge.

	Cs in 0.1 M $TBAPF_6$	Cs in 1 M $TBAPF_6$	Pb in 0.1 M $TBAPF_6$	Pb in 1 M $TBAPF_6$
SD	0.03558	0.00308	0.05208	0.01893
RSD%	0.6	1.8	0.8	3.7

Table S3. Percentage of different phases of $CsPbBr_3$ electrode before and after 500, 1000, 2000, and 10000 cycles.

	0.1 M $TBAPF_6$	0	500	1000	2000	1 M $TBAPF_6$	10000
Cubic%		89	85.37	82.8	67.53		86.32
Orthorhombic%		11	10.1	9.8	7.99		9.67
$CsPF_6$%		0	4.53	7.4	24.48		4.01
RWP		4.43	6.29	5.89	5.56		7.48
GOF		1.26	1.81	1.24	1.75		1.43

REFERENCE

1. He X, Qiu Y, Yang S. Fully-Inorganic Trihalide Perovskite Nanocrystals: A New Research Frontier of Optoelectronic Materials. *Advanced materials (Weinheim)* 2017;29:1700775-n/a. DOI: 10.1002/adma.201700775.

2. Jiang G, Guhrenz C, Kirch A, Sonntag L, Bauer C, Fan X, et al. Highly Luminescent and Water-Resistant CsPbBr3–CsPb2Br5 Perovskite Nanocrystals Coordinated with Partially Hydrolyzed Poly(methyl methacrylate) and Polyethylenimine. *ACS Nano* 2019;13:10386-96. DOI: 10.1021/acsnano.9b04179.

3. Ling X, Yuan J, Zhang X, Qian Y, Zakeeruddin S M, Larson B W, et al. Guanidinium-Assisted Surface Matrix Engineering for Highly Efficient Perovskite Quantum Dot Photovoltaics. *Advanced Materials* 2020;32:2001906. DOI: https://doi.org/10.1002/adma.202001906.

4. Zhang M, Zheng Z, Fu Q, Chen Z, He J, Zhang S, et al. Growth and characterization of all-inorganic lead halide perovskite semiconductor CsPbBr3 single crystals. *CrystEngComm* 2017;19:6797-803. DOI: 10.1039/C7CE01709J.

5. Algadi H, Mahata C, Woo J, Lee M, Kim M, Lee T. Enhanced Photoresponsivity of All-Inorganic (CsPbBr3) Perovskite Nanosheets Photodetector with Carbon Nanodots (CDs). *Electronics (Basel)* 2019;8:678. DOI: 10.3390/electronics8060678.

6. Zhao M, Shi Y, Dai J, Lian J. Ellipsometric study of the complex optical constants of a CsPbBr3 perovskite thin film. *Journal of materials chemistry C, Materials for optical and electronic devices* 2018;6:145-1455. DOI: 10.1039/c8tc03222j.

7. Chen H, Wang Y, Wang J, Liu W. Thermal Stability of CsPbBr3 Perovskite Quantum Dots Assembled with SBA-15. *Coatings (Basel)* 2021;11:953. DOI: 10.3390/coatings11080953.

8. Guan Z, Wu Y, Wang P, Zhang Q, Wang Z, Zheng Z, et al. Perovskite photocatalyst CsPbBr3-xIx with a bandgap funnel structure for H2 evolution under visible light. *Applied catalysis B, Environmental* 2019;245:522-7. DOI: 10.1016/j.apcatb.2019.01.019.

9. Yuan B, Li N, Liu J, Xu F, Li C, Juan F, et al. Improving the performances of CsPbBr3 solar cells fabricated in ambient condition. *Journal of materials science Materials in electronics* 2020;31:21154-67. DOI: 10.1007/s10854-020-04627-6.

10. Zhang M, Tian Z-Q, Zhu D-L, He H, Guo S-W, Chen Z-L, et al. Stable CsPbBr3 perovskite quantum dots with high fluorescence quantum yields. *New journal of chemistry* 2018;42:9496-500. DOI: 10.1039/C8NJ01191E.

11. Liu M, Zhong G, Yin Y, Miao J, Li K, Wang C, et al. Aluminum-Doped Cesium Lead Bromide Perovskite Nanocrystals with Stable Blue Photoluminescence Used for Display Backlight. *Advanced science* 2017;4:1700335-n/a. DOI: 10.1002/advs.201700335.

12. Li M, Zhang X, Matras-Postolek K, Chen H-S, Yang P. An anion-driven Sn2+ exchange reaction in CsPbBr3 nanocrystals towards tunable and high photoluminescence. *Journal of materials chemistry C, Materials for optical and electronic devices* 2018;6:5506-13. DOI: 10.1039/C8TC00990B.

13. Maji P, Ray A, Sadhukhan P, Roy A, Das S. Fabrication of symmetric supercapacitor using cesium lead iodide (CsPbI3) microwire. *Materials Letters* 2018;227:268-71. DOI: https://doi.org/10.1016/j.matlet.2018.05.101.

14. Popoola I, Gondal M, Oloore L, Popoola A, AlGhamdi J. Fabrication of organometallic halide perovskite electrochemical supercapacitors utilizing quasi-solid-state electrolytes for energy storage devices. *Electrochimica Acta* 2020;332:135536. DOI: https://doi.org/10.1016/j.electacta.2019.135536.

15. Zhou S, Li L, Yu H, Chen J, Wong C-P, Zhao N. Thin Film Electrochemical Capacitors Based on Organolead Triiodide Perovskite. *Advanced Electronic Materials* 2016;2:1600114. DOI: https://doi.org/10.1002/aelm.201600114.

16. Pious J K, Lekshmi M L, Muthu C, Rakhi R B, Vijayakumar C. Zero-Dimensional Methylammonium Bismuth Iodide-Based Lead-Free Perovskite Capacitor. *ACS Omega* 2017;2:5798-802. DOI: 10.1021/acsomega.7b00973.

17. Li T, Mallows J, Adams K, Nichol G S, Thijssen J H J, Robertson N. Thiourea Bismuth Iodide: Crystal Structure, Characterization and High Performance as an Electrode Material for Supercapacitors. *Batteries & Supercaps* 2019;2:568-75. DOI: https://doi.org/10.1002/batt.201900005.